Zonally Symmetric Adjustment in the Presence of Artificial Relaxation

PETER HITCHCOCK AND PETER H. HAYNES

Department of Applied Mathematics and Theoretical Physics, University of Cambridge, Cambridge, United Kingdom

(Manuscript received 12 January 2014, in final form 15 June 2014)

ABSTRACT

Numerical experiments, presented in a companion paper, have been performed in which the zonal-mean state of the stratosphere in a comprehensive, stratosphere-resolving, general circulation model is strongly relaxed (or ''nudged'') toward the evolution of a reference sudden warming event in order to investigate its influence on the freely evolving troposphere below. Similar approaches have been used in a number of other studies. This raises the question of whether such an artificial relaxation induces the adiabatic and diabatic adjustments expected below the region of nudging, even in the absence of the stratospheric wave driving responsible for the reference event.

Motivated by this question, the zonally symmetric quasigeostrophic diabatic response to zonal forces (representing wave driving) in a system nudged to a time-dependent reference state is studied. In the presence of wave driving in the nudging region that differs from the reference state, the meridional mass circulation of the reference state is reproduced only in the region below the nudging up to a correction that is inversely proportional to the strength of the nudging. The anomalous circulation is confined because of an effective boundary condition at the interface of the nudging layer. The nudging also produces an artificial ''sponge-layer feedback'' immediately below the region of the nudging in response to differences in the tropospheric wave driving. The strength of this artificial feedback is closely related to the strength of the effective boundary condition; however, the time scale required for the sponge-layer feedback to be established is typically much longer than that required for the confinement.

1. Introduction

Numerical studies of the atmospheric general circulation impose linear relaxational terms on both the thermodynamic and momentum equations for a variety of reasons. In simplified models, linear, local relaxation of the temperature field toward a notional radiative equilibrium state is a useful (e.g., Held and Suarez 1994) simplification of diabatic heating. Similarly, relaxation of the wind field can be used to parameterize boundary layer friction near the surface, and as a sponge layer or a crude parameterization of gravity wave drag in the stratosphere (e.g., Taguchi et al. 2001; Polvani and Kushner 2002). Thermal or mechanical relaxation is sometimes used in more comprehensive models to artificially induce features of the general circulation not properly simulated by the free-running model such as the quasibiennial oscillation (Morgenstern et al. 2010), or as a simple form of data assimilation [e.g., the REF-C1SD simulations specified in Eyring et al. (2013)]. To distinguish them from physical processes, such artificial relaxation will be referred to here as ''nudging.'' Mechanical nudging in particular, having no physical counterpart in the free troposphere or stratosphere, can introduce spurious sources or sinks of angular momentum, which in turn have been shown to produce spurious nonlocal responses (Shepherd et al. 1996; Shepherd and Shaw 2004).

Another use of nudging is for process-based studies, which seek to isolate the role of some component of the general circulation by artificially constraining its state toward some prespecified, possibly time-dependent, reference state, while leaving another component of the atmosphere free in order to understand the influence of the former on the latter (Alexandru et al. 2009; Bielli et al. 2010; Hoskins et al. 2012). In particular, a number of recent studies have constrained the stratosphere in order to better understand its role in seasonal prediction (Douville 2009; Jung et al. 2010) and its effect on tropospheric variability (Simpson et al. 2011, 2013a,b). Using a methodology closely related to the Simpson et al. studies, the companion paper by Hitchcock and

Corresponding author address: Peter Hitchcock, Dept. of Applied Mathematics and Theoretical Physics, Centre for Mathematical Sciences, Wilberforce Road, Cambridge CB3 0WA, United Kingdom.
E-mail: aph42@cam.ac.uk

DOI: 10.1175/JAS-D-14-0013.1

Simpson (2014, hereafter HS) has examined the downward influence of sudden warmings on the tropospheric state by relaxing the zonal-mean state in the stratosphere toward a reference state that is the time-evolving zonal mean of a freely simulated warming. Because of the potential for nudging to produce spurious responses, it is essential to fully understand the impact of the artificial relaxation terms imposed in the stratosphere in order to properly interpret the implications of these studies.

To be specific, the planetary wave driving in the stratosphere responsible for the breakdown of the Arctic polar vortex during a sudden warming is known to influence the tropospheric winds directly through the meridional circulation that it induces, both due to the stratospheric potential vorticity anomalies (Hartley et al. 1998) and through further zonally symmetric diabatic feedbacks (Haynes et al. 1991) that reinforce the downward influence (Song and Robinson 2004; Thompson et al. 2006). If, as in HS, the eddies are not also relaxed toward those in the reference state, it is unlikely that the nudged simulations will exhibit the same amplification of the stratospheric waves seen in the reference warming, and the deceleration of the zonal wind in the stratosphere will be induced instead primarily by the artificial relaxation. In this case, it is not immediately clear that the nudging will induce the same meridional circulation in the troposphere as did the original wave driving [particularly if, as in HS, the relaxation is imposed on both the horizontal wind field and the temperatures with equal strengths, a special case highlighted by Plumb (1982)]. It is not sufficient to argue this, for instance, on the basis of potential vorticity inversion and the assumption that the nudging will reproduce the zonal-mean potential vorticity field of the reference state within the nudging region, since the adjustment of the system is diabatic even outside the region of the nudging (Haynes et al. 1991). This argument would also suggest that the nudging would reproduce the meridional circulation of the reference state within the nudging region itself, which is shown below not to be the case.

A second issue is that the presence of mechanical nudging aloft can produce spurious responses even in response to torques applied below the region of relaxation, an effect termed a ''sponge-layer feedback'' by Shepherd et al. (1996). This arises when part of the meridional circulations induced by the torque close upward, since the nudging permits return flow across angular momentum contours even in the steady state. The effect results in wind and temperature anomalies just below the base of the nudging region that can be, in the worst case, as large as the physical wind and temperature response at the level of the applied torque.

In fact, the experiments in HS produce a tropospheric response that closely resembles composites of observed sudden warmings. To correctly interpret these results, it is therefore of central importance to understand the nature of the meridional circulations induced by the nudging and to establish whether the response obtained by HS is physical or spurious.

We consider both of these issues (that of the downward influence of the nudging and of the spurious sponge-layer feedback) here within the idealized context of a quasi-geostrophic model on the sphere, which is simple enough to make some analytical progress. Despite the assumption of simple thermal wind balance inherent in this model, it has been shown to reproduce the zonal-mean evolution of the stratospheric anomalies during a sudden warming to a good approximation (Hitchcock and Shepherd 2013). Both issues can be conveniently described by considering the effects of the anomalous wave driving $\mathcal{F}'$; that is, the difference between the wave driving in the nudged simulation and that in the reference state to which the nudging is relaxing. The behavior of the nudging layer is controlled by two key dimensionless parameters: K, the ratio of mechanical to thermal relaxation rates within the nudging layer, and A, the ratio of the thermal relaxation rate within the nudging layer and the radiative relaxation rate relevant in the free atmosphere.

We show that, while the meridional mass circulation within the nudging region itself is only weakly controlled by the nudging, the mass circulation in the free region below is suppressed by strong nudging ($A \gg 1$) so long as $K > 0$. The boundary between the nudged and free regions acts as an effective barrier to the mass circulation, such that the majority of the response to $\mathcal{F}'$ is confined within the nudging region. In this case, the anomalous zonal winds and temperatures will also be strongly constrained by the relaxation throughout the depth of the atmosphere; with the temperatures controlled primarily by the parameter A and the winds by the combination $A\sqrt{K}$. The presence of a frictional lower boundary somewhat reduces the efficiency of this confinement, but this effect decays exponentially with the distance between the nudging and the frictional layers.

However, the strength of the confinement of the mass circulation within the nudging layer is closely related to the strength of the sponge-layer feedback, such that in steady state, the stronger the confinement, the stronger the sponge-layer feedback, although the time scales on which the two effects are established differ. The presence of a frictional lower boundary has a greater effect on the sponge-layer feedback, reducing its magnitude.

The calculations described here amount to a relatively straightforward extension of the zonally symmetric adjustment to downward control described by Haynes et al. (1991) to include mechanical relaxation and are closely related to the sponge-layer feedback calculations

of Shepherd et al. (1996). A general framework for considering the influence of nudging toward a reference state within a quasigeostrophic framework is introduced in section 2. This is then developed within a context relevant for HS in section 3 and applied in section 4 explicitly to their experimental results to show that, while spurious, nonphysical effects are likely to be present, they are negligible compared to the response obtained and amount to a small correction. Finally, conclusions and a brief discussion of the choice of parameters for nudging studies are presented in section 5. The primary aim of this paper is to support HS and similar investigations, and the analysis presented in section 3 is deliberately kept concise and is restricted to solutions for steady-state and oscillatory forcings. However, it can be developed further to describe the transient adjustment to the steady state and this is included in the appendix to this paper.

2. Model setup

The starting point is the zonally symmetric quasigeostrophic equations in log-pressure height on the sphere (Plumb 1982):

$$\partial_t u - 2\Omega \sin\phi v = \mathcal{F} - k(z)u, \tag{1a}$$

$$\partial_t T + \frac{H}{R} N^2 w = \mathcal{H} - \alpha(z)T, \tag{1b}$$

$$\frac{\partial_\phi(\cos\phi v)}{a\cos\phi} + \frac{\partial_z(\rho_0 w)}{\rho_0} = 0, \tag{1c}$$

$$2\Omega \sin\phi \partial_z u = -\frac{R}{aH}\partial_\phi T. \tag{1d}$$

All quantities are independent of longitude. The zonal wind u and temperature T are at all times in thermal wind balance [(1d)], which is maintained by the nondivergent meridional mass circulation $\rho_0 v$, $\rho_0 w$ with corresponding streamfunction Ψ. The background density ρ_0 decays with scale height H. The terms Ω and a are the angular velocity and radius of Earth, respectively; N is the buoyancy frequency; and R is the specific gas constant for dry air. All external forcings (including eddy fluxes of momentum and heat) are included in the mechanical ($\mathcal{F}$) and thermal ($\mathcal{H}$) forcing terms.

This set describes both the direct Eulerian (EM) and the transformed Eulerian (TEM) mean formulations, with appropriate changes in the specification of the eddy forcings and the lower-boundary condition; however, we work primarily within the TEM framework, in which we can identify $\mathcal{F}$ as the convergence of the Eliassen–Palm flux and the thermal forcing $\mathcal{H}$ due to eddy fluxes vanishes. The mechanical (k) and thermal (α) relaxation coefficients (as well as N^2) are taken to be functions of the log-pressure height only, so that the equations admit separable solutions (Plumb 1982). This gives rise to an eigenvalue problem in the meridional direction whose solutions are zero-wavenumber, zero-frequency Hough functions. The constant of separation ϵ_n is negative for all n. The gravest meridional mode corresponds to $n = 1$, and the characteristic meridional length scale of the modes decreases as n (and $|\epsilon_n|$) increases (see Table 1). Projecting all fields on to the appropriate eigenfunctions yields the following set:

TABLE 1. Values of the nondimensional parameters ϵ_n and b_n and the Rossby height H_R (see text) for the first six meridional modes with $\Omega = 7.29 \times 10^{-5}\,\mathrm{s}^{-1}$, $a = 6.371 \times 10^6\,\mathrm{m}$, $N^2 = 4 \times 10^{-4}\,\mathrm{s}^{-2}$, and $H = 7 \times 10^3\,\mathrm{m}$.

n	ϵ_n	b_n	H_R (km)
1	−8.127	0.185	16.3
2	−12.54	0.285	13.1
3	−35.42	0.805	7.80
4	−44.73	1.02	6.94
5	−82.38	1.87	5.12
6	−96.61	2.19	4.73

$$\partial_t u_n - 2\Omega v_n = \mathcal{F}_n - k(z)u_n, \tag{2a}$$

$$\partial_t T_n + \frac{H}{R} N^2 w_n = \mathcal{H}_n - \alpha(z)T_n, \tag{2b}$$

$$\frac{v_n}{a} + \frac{\partial_z(\rho_0 w_n)}{\rho_0} = 0, \tag{2c}$$

$$2\Omega a \partial_z u_n = -\frac{R}{H}\epsilon_n T_n. \tag{2d}$$

The mass streamfunction, given by $\Psi_n = \rho_0 w_n$, will also be useful. The full meridional dependence can be recovered by solving this set for each Hough mode independently; however, to keep the notation simple, we now drop the subscript n from all quantities except the constant ϵ_n and the related nondimensional quantity $b_n = (H/H_R)^2$, where the Rossby height is defined as $H_R = 2\Omega a(-\epsilon_n N^2)^{-1/2}$. Values of ϵ_n and b_n for the first few meridional modes relevant to Earth's stratosphere are given in Table 1.

Solving this set for u,

$$(\partial_t + k)u - \frac{1}{\rho_0}\partial_z[H_R^2 \rho_0 (\partial_t + \alpha)\partial_z u] = \mathcal{F}. \tag{3}$$

Other relevant fields can be computed from solutions to (3). Most usefully within the present context, the temperature and the vertical velocity are given by

$$T = -\frac{2\Omega a}{\epsilon_n}\frac{H}{R}\partial_z u, \tag{4}$$

$$w = -\frac{H_R^2}{2\Omega a}(\partial_t + \alpha)\partial_z u. \tag{5}$$

Given appropriate boundary conditions, the linear operator on the left-hand side of (3) can be inverted, so that the response of the zonal wind to a time-dependent forcing can be written as

$$u(z,t) = \int_{-\infty}^{t}\int_{-\infty}^{\infty} B(z,z',t-\tau;\alpha,k)\mathcal{F}(z',\tau)\,dz'\,d\tau, \tag{6}$$

where B depends in particular on the profiles of the mechanical and thermal relaxation.

Three systems are of interest: the reference state, the nudged simulation that is relaxed to the former, and the difference between the two. We define first the reference state (u_0, T_0, w_0, etc.), which we take to be a freely evolving solution to this set of equations in the sense that no artificial nudging is imposed, though physical relaxational processes (such as radiative heating and surface friction) are represented by some profile of $\alpha(z)$ and $k(z)$. We consider this system to be driven by a time-dependent zonal force $\mathcal{F}_0$, though more generally a nonrelaxational heating $\mathcal{H}_0$ could be considered as well.

The nudged simulation (u_N, T_N, w_N, etc.) is modeled by the same set of equations but subject to additional terms relaxing the stratosphere toward the reference state: $-k_r(z)(u_N - u_0)$ on the right-hand side of (1a) and $-\alpha_r(z)(T_N - T_0)$ on the right-hand side of (1b). It is driven by a different time-dependent force $\mathcal{F}_N$, which need not bear any resemblance to $\mathcal{F}_0$.

As mentioned above, it is useful to consider the behavior of the anomalous circulation in the nudged simulation, that is, the difference between the nudged simulation and the reference state $u' = u_N - u_0$ (with similar definitions for T', w', etc.). This satisfies

$$(\partial_t + k + k_r)u' - \frac{1}{\rho_0}\partial_z[H_R^2\rho_0(\partial_t + \alpha + \alpha_r)\partial_z u'] = \mathcal{F}',$$
$$\mathcal{F}' = \mathcal{F}_N - \mathcal{F}_0, \tag{7}$$

which is identical to (3) but with modified diabatic relaxation. If the anomalous zonal force $\mathcal{F}'$ vanishes, no anomalous circulation will be present, and the nudged simulation will match the reference state. A mild assumption, which is essentially already implied by the quasigeostrophic scaling, has been made that the background static stability is constant in height and does not change in the nudged simulation. The evolution of the anomalous zonal wind can then be written as

$$u' = \int_{-\infty}^{t}\int_{-\infty}^{\infty} B(z,z',t-\tau;\alpha+\alpha_r,k+k_r)\mathcal{F}'(\tau)\,d\tau, \tag{8}$$

Note that while we have assumed here that the damping coefficients vary only with height so that the set (1) admits separable equations, the character of the anomalous circulation does not require this assumption, and a result analogous to (8) holds for other nudging geometries.

Within the context of experiments studying stratosphere–troposphere coupling, we are most interested in the winds induced throughout the atmosphere by stratospheric wave driving, as a result of the nonlocality of B. One central issue to be addressed in this paper is the nature of the differences between the winds induced by the stratospheric wave driving (defined by some appropriate projection operator) in the reference simulation $\mathcal{F}_{0,s}$ and those induced by the combination of wave driving $\mathcal{F}_{N,s}$ and nudging in the nudged simulation. Because B is linear, the anomalous wind driven by these differences in stratospheric wave driving can be written as

$$u'_s = \int_{-\infty}^{t}\int_{-\infty}^{\infty} B(z,z',t-\tau;\alpha+\alpha_r,k+k_r)\mathcal{F}'_s(\tau)\,d\tau,$$
$$\mathcal{F}'_s = \mathcal{F}_{N,s} - \mathcal{F}_{0,s}. \tag{9}$$

Any such anomalous winds will be produced by the differences in the stratospheric wave driving in the nudged run and the reference run, and in the case that this wave driving is identical, $\mathcal{F}'_s = 0$ and $u'_s = 0$, so the induced tropospheric winds in the nudged simulation will match those of the reference simulation.

A second central question is whether the presence of the nudging region will affect the response of the system to wave driving outside the region of nudging. For instance, again within the context of HS, the stratospheric anomalies associated with the sudden warming are shown to produce a response in the tropospheric eddies. As in the case just described, if the torque produced by these tropospheric eddies is identical to that produced by the eddies in the reference state, then the nudging will have no effect and the response will be just as in the reference state. Since, however, there is substantial internal tropospheric variability, one expects that over a large ensemble of nudged simulations, the ensemble-averaged wave driving will differ significantly from the single realization of the reference state. The question in this case can be posed again just as above, except in this case the anomalous forcing is below the region of the nudging.

3. Results

To quantify the spurious effects of the nudging in the experiments of HS, it is, therefore, informative to study

the response to a forcing in an idealized nudging layer with the understanding that the response in this idealization represents the anomalous circulation produced in the nudged simulation due to the mismatch $\mathcal{F}'$ in the wave driving between the nudged and the reference simulations.

a. Response in an unbounded atmosphere

To begin, we consider the response to oscillatory, delta function forcing centered at z_F with the meridional structure of the nth Hough mode: $\mathcal{F}' = f_n'\delta[(z - z_f)/H]\exp(i\omega t)$. To simplify the problem, we consider an atmosphere of infinite depth and take as vertical boundary conditions that all mass-weighted fields decay both above and below. The mechanical and thermal relaxation terms are taken to be constant in height, but otherwise are unspecified; at this stage, they may be physical or artificial. The zonal wind response is

$$u' = U^+ \exp\left(\frac{\Lambda^+|z - z_f|}{H}\right) \quad \text{if} \quad z > z_f, \tag{10a}$$

$$\rho_0 u' = \rho_0(z_f)U^- \exp\left(\frac{\Lambda^+|z - z_f|}{H}\right) \quad \text{if} \quad z < z_f, \tag{10b}$$

in which

$$\Lambda^{\pm}(i\omega) = \frac{1}{2} \mp \frac{1}{2}\sqrt{1 + 4b_n}\left(\frac{i\omega + \tilde{\alpha}}{i\omega + \alpha}\right)^{1/2}, \tag{11}$$

$$U^{\pm}(i\omega) = \frac{f_n' b_n}{i\omega + \alpha}\frac{1}{\Lambda^- - \Lambda^+}, \tag{12}$$

and

$$\tilde{\alpha} = \alpha\frac{1 + 4b_n K}{1 + 4b_n}, \quad K = \frac{k}{\alpha}. \tag{13}$$

The ratio K of mechanical to thermal relaxation rates will be central in the following analysis.

From (4) and (5), the response of the temperature and the vertical velocity have the same structure as (10), but with prefactors

$$T^{\pm}(i\omega) = \frac{H}{R}\frac{f_n' N^2 H}{2\Omega a}\frac{1}{i\omega + \alpha}\frac{\Lambda^{\pm}}{\Lambda^- - \Lambda^+}, \tag{14}$$

$$w^{\pm}(i\omega) = \frac{f_n' H}{2\Omega a}\frac{\Lambda^{\pm}}{\Lambda^- - \Lambda^+}. \tag{15}$$

These solutions have been discussed by Garcia (1987) and Dunkerton (1989). However, some of their properties are worth reviewing within the present context. In the high-frequency, adiabatic limit, the problem becomes equivalent to that of Eliassen (1951), and the e-folding height $H/\Lambda^+(i\omega)$ tends to

$$H/\Lambda^+(i\infty) \equiv H_E = \frac{2H}{\sqrt{1 + 4b_n} - 1}, \tag{16}$$

while, in steady state, it depends on the ratio K:

$$H/\Lambda^+(0) \equiv H_K = \frac{2H}{\sqrt{1 + 4b_n K} - 1}. \tag{17}$$

For equal rates of thermal and mechanical relaxation, $H_K = H_E$. For sufficiently small $b_n K$, which, for $K \approx 1$, is only relevant for the gravest meridional modes (Table 1), H_K tends to $H_R^2(HK)^{-1}$, while for sufficiently large $b_n K$, it tends to $H_R K^{-1/2}$. The larger the ratio K is, the more vertically confined the response is to levels near the forcing, and this confinement is stronger at shorter meridional length scales. If $K = 0$, this steady-state length scale diverges and the frictionless case considered by Haynes et al. (1991) is recovered.

In the steady state, the prefactors of the zonal wind, temperature, and vertical velocity become, respectively,

$$U^{\pm} = \frac{f_n' b_n}{\alpha}(1 + 4b_n K)^{-1/2}, \tag{18}$$

$$T^{\pm} = \frac{H}{R}\frac{f_n' H}{2\Omega a}\frac{N^2}{\alpha}\frac{(1 + 4b_n K)^{-1/2} \mp 1}{2}, \quad z \gtrless z_f, \tag{19}$$

$$w^{\pm} = \frac{f_n' H}{2\Omega a}\frac{(1 + 4b_n K)^{-1/2} \mp 1}{2}, \quad z \gtrless z_f. \tag{20}$$

In all cases, these prefactors scale with f_n'. In the case of large $b_n K$, the magnitude of the zonal wind response is inversely proportional to the geometric mean of the mechanical and thermal relaxation rates, while in the case where $b_n K$ is small, it is controlled by the thermal relaxation alone.

The magnitude of the temperature response is primarily controlled by the thermal relaxation alone, exhibiting only a weak dependence on K, which plays a role in determining the ratio of the response above and below the level of the forcing.

In contrast, the magnitude of the vertical velocities scales only weakly with the relaxation, which plays a role only through K, and determines the ratio of the circulation above and below the level of the forcing.

If we consider parameters relevant for the interior of the nudging layer, within the context of which it is desirable to minimize the strength of this anomalous

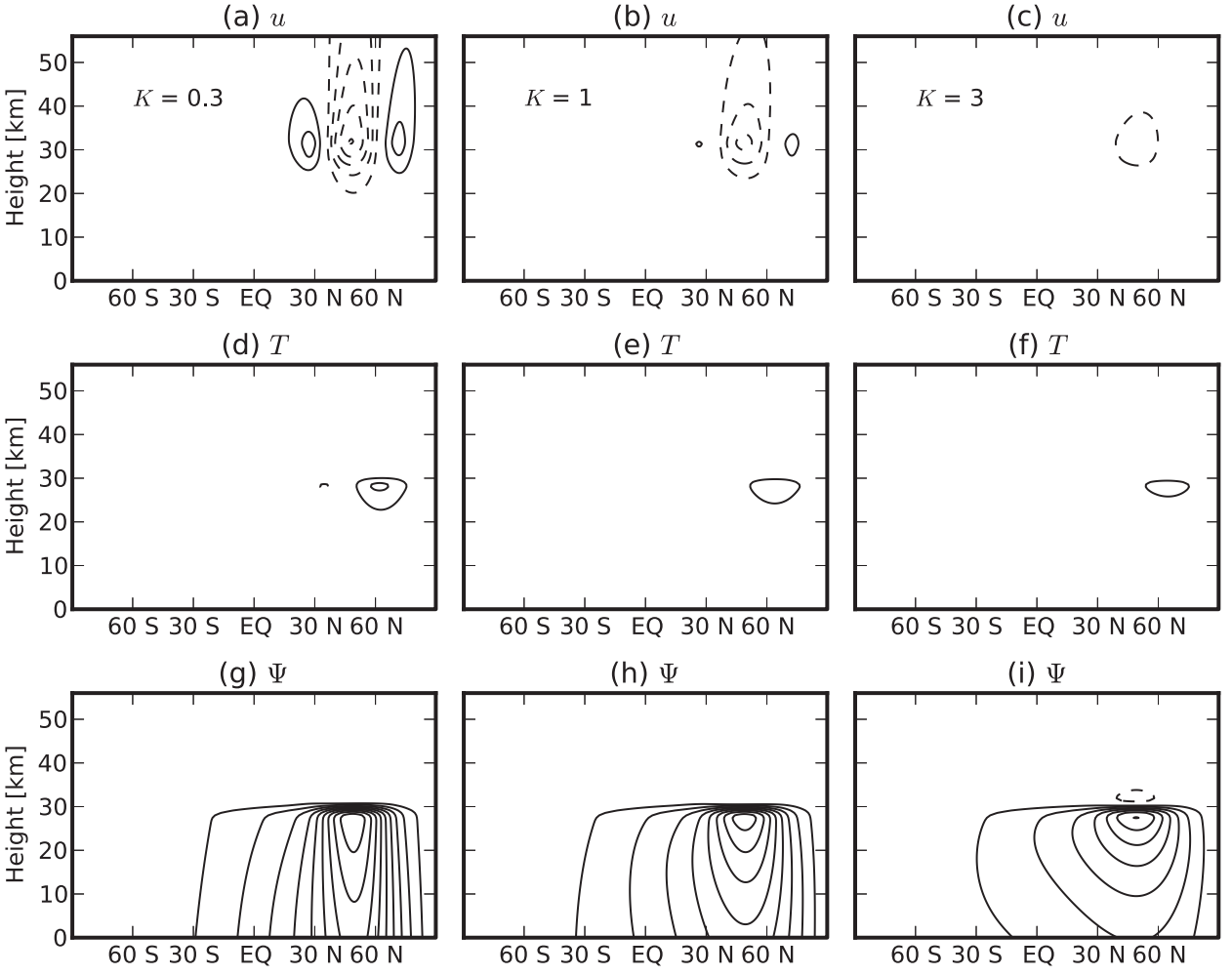

FIG. 1. Steady-state response to an extratropical force of order $-5\,\mathrm{m\,s^{-1}\,day^{-1}}$ in an unbounded atmosphere with a thermal relaxation rate of $4\,\mathrm{day^{-1}}$ for three values of K. See text for the details of the forcing. (a)–(c) The zonal wind response with contour interval of $0.02\,\mathrm{m\,s^{-1}}$. (d)–(f) The temperature response with contour interval of 0.02 K. (g)–(i) The meridional mass circulation response with contour interval of $5\,\mathrm{kg\,m^{-1}\,s^{-1}}$. The origin of the height scale on the left indicates where the density field has a value of $1.47\,\mathrm{kg\,m^{-3}}$. The zero contours in these and subsequent plots have been omitted.

circulation, increasing the strength of a vertically uniform artificial relaxation will not directly control the strength of the anomalous meridional circulation produced by any anomalous wave driving. The larger the ratio K is, however, the more vertically confined this anomalous circulation will be.

These steady-state responses are illustrated in Fig. 1. The forcing applied is of the form

$$\mathcal{F}' = \begin{cases} \dfrac{fH}{\sqrt{2\pi\sigma_z^2}} \exp\left[-\dfrac{(z-z_0)^2}{\sigma_z^2}\right] \cos^2\left[\dfrac{\pi(\phi-\phi_0)}{2\sigma_\phi}\right], & \text{if} \quad |\phi-\phi_0| < \sigma_\phi \\ 0, & \text{otherwise}, \end{cases} \tag{21}$$

where $f = -5\,\mathrm{m\,s^{-1}\,day^{-1}}$, $z_0 = 30\,\mathrm{km}$, $\sigma_z = 1\,\mathrm{km}$, $\phi_0 = 50°\mathrm{N}$, and $\sigma_\phi = 25°$; the solutions are computed by latitudinal decomposition into Hough functions and a standard Green's function method. The three columns correspond to three values of K: 0.3, 1, and 3. In all cases, $\alpha = 4\,\mathrm{day^{-1}}$. The absolute height is only relevant for the mass streamfunction, for which the density field is defined to be equal to $1.47\,\mathrm{kg\,m^{-3}}$ at $z = 0\,\mathrm{km}$. The

amplitude of the zonal wind response is about 3 times weaker when K is 3 than it is when K is 0.3, while the temperature and mass streamfunction are much less sensitive to K. As K increases, H_K decreases, and the response in all variables becomes more confined near the height of the forcing. The $K = 1$ streamfunction response is identical to the high-frequency adiabatic response since $\Lambda^{\pm}$ are independent of frequency in this case. The spatial structures of the zonal wind and temperature fields at $K = 1$ correspond to their respective tendencies in the adiabatic case [cf. (16) and (17)].

b. Nudging above a free layer

We turn now to the case with two semi-infinite regions: a region of strong nudging above a "free" region, subject only to thermal relaxation. The boundary between the two regions is taken to be at z_N. The discontinuity in the solution at z_N is in the first derivative of the zonal winds, deduced from the condition that the integral of (3) over a neighborhood of z_N vanishes; specifically,

$$(\partial_t + \alpha_N)\partial_z u'|_{z_N^+} = (\partial_t + \alpha_F)\partial_z u'|_{z_N^-}. \tag{22}$$

It may also be deduced that u' is continuous across z_N. From (5), this implies that the mass circulation is also continuous across this boundary. The subscripts N and F on α and k (and parameters such as K, $\Lambda^{\pm}$, and $U^{\pm}$ that depend on them) denote the rates appropriate for the nudging layer and the free layer, respectively. Note that the rate α_N corresponds to the net thermal relaxation within the nudging layer; if α_F corresponds to the physical thermal relaxation acting throughout the atmosphere, $\alpha_N = \alpha_r + \alpha_F$.

In the case that the forcing is taken to be oscillatory and within the nudging layer ($z_f > z_N$), the solution above z_N consists of that given above for the unbounded, single-layered case, plus a correction to the zonal wind:

$$u_2' = U_N^+ \exp\left(\frac{\Lambda_N^+|z - z_N|}{H}\right) C_+ \exp\left(-\frac{\Lambda_N^-|z_f - z_N|}{H}\right), \tag{23}$$

with

$$C_+ = \frac{(i\omega + \alpha_F)\Lambda_F^- - (i\omega + \alpha_N)\Lambda_N^-}{(i\omega + \alpha_N)\Lambda_N^+ - (i\omega + \alpha_F)\Lambda_F^-}. \tag{24}$$

Similar corrections hold for the temperature and vertical velocity, with the corresponding prefactors. The correction is largest near z_N, and in the steady state it falls off with height above the boundary, with an e-folding scale of H_{K_N}. The factor C_+ becomes

$$C_+ = \frac{A - 1 + (1/2)A(\sqrt{1 + 4b_n K_N} - 1)}{1 + (1/2)A(\sqrt{1 + 4b_n K_N} - 1)}, \tag{25}$$

which tends to 1 as $b_n K_N$ gets large, and to $A - 1$ as $b_n K_N$ goes to zero, where $A = \alpha_N/\alpha_F$ is the ratio between the thermal relaxation rates in the nudging layer and the free layer.

Below the nudging region, the mass-weighted zonal wind is

$$\rho_0 u' = \rho_0(z_f) U_F^- \times \exp\left(\frac{\Lambda_F^+|z - z_N|}{H}\right) C_- \exp\left(\frac{\Lambda_N^+|z_f - z_N|}{H}\right), \tag{26}$$

with

$$C_- = \frac{(i\omega + \alpha_F)(\Lambda_F^- - \Lambda_F^+)}{(i\omega + \alpha_F)\Lambda_F^- - (i\omega + \alpha_N)\Lambda_N^+}, \tag{27}$$

and again similar expressions hold for the temperature and vertical velocity. By comparison with (10b), the influence of the nudging layer is encoded in the factor C_- and the additional exponential factor. As with the correction term within the nudging region, the mass-weighted response below the nudging boundary decays with the distance of the forcing from the nudging boundary, with a steady-state e-folding scale of H_{K_N}. In the steady state, Λ_F^+ vanishes, and the mass-weighted fields remain constant with height below z_N. Unlike the zonal and vertical winds, the temperatures are not continuous across z_N, since they must adjust more immediately below the interface between the two regions than just above to balance the same adiabatic heating.

The factor C_- thus dictates the response of all fields within the free layer, including that of the mass circulation. In the steady state,

$$C_- = \frac{1}{1 + (1/2)A(\sqrt{1 + 4b_n K_N} - 1)}. \tag{28}$$

If K_N is 0, then this goes to 1 for any A and n. However, if K_N is not zero, then for sufficiently large n this will tend to $(A\sqrt{b_n K_N})^{-1}$.

This implies that, even for anomalous wave driving very close to the boundary between the nudging region and the free region, the anomalous meridional circulation within the free region will remain small,

controlled by the strength of the nudging. This stands in contrast to the case considered above, where within an unbounded nudging region, the strength of the nudging exerts only a weak control on the magnitude of the meridional circulation. This confinement can be understood as a consequence of the steady-state version of (22), which, since $\Lambda_F^- = 1$ when $\omega = 0$, implies that the vertical shear just above the interface between the nudging layer and the free layer below is given by

$$\partial_z u'(z_N + \epsilon) = \frac{u'(z_N - \epsilon)}{AH} = \frac{u'(z_N + \epsilon)}{AH}, \tag{29}$$

since u' is continuous through z_N. The vertical velocity at the lower boundary of the nudging layer is thus given by

$$w'(z_N + \epsilon) = -\frac{H}{2\Omega a}\frac{\alpha_F u'(z_N + \epsilon)}{b_n}, \tag{30}$$

and if the anomalous zonal winds scale with $b_n(\alpha_N\sqrt{b_n K_N})^{-1}$ within the nudging layer, then the vertical wind at the base of the nudging layer must scale as $(A\sqrt{b_n K_N})^{-1}$, which is smaller by a factor of A than typical values of w within the nudging layer as estimated by (15). Note that this argument fails if $K_N = 0$, in which case u' within the nudging layer is no longer controlled by α_N but instead by the profile of the radiative relaxation below the level of the forcing. This can be seen in the steady-state downward control limit:

$$u'(z) = \int_{-\infty}^{z} \frac{f_n' b_n}{\alpha(z')}\frac{\rho_0(z_f)}{\rho_0(z')}\frac{dz'}{H}, \quad z < z_f. \tag{31}$$

In the present setup this nonlocal contribution to u' arises from the correction u_2'.

The overall steady-state response is illustrated in Fig. 2 for the same forcing considered in Fig. 1. The thermal relaxation in the free region is set to $\alpha_F = 0.1\ \text{day}^{-1}$, which corresponds to $A = 40$. As discussed, the mass circulation closes mostly within the nudging region, with only a small component penetrating into the free region, in strong contrast with the mass circulation shown in Fig. 1. The confinement strengthens as K_N increases. For small K_N, the zonal wind response within the nudged region is larger in the presence of a free layer below, consistent with the behavior of C_+. The discontinuity in the temperature field at z_N is also more apparent for smaller K_N.

While the emphasis here has been on the steady-state and purely oscillatory responses, a discussion of the transient response to a switch-on forcing is given in the appendix.

c. Forcing within the free region

As discussed in the previous section, the sponge-layer feedback can be described by considering the response of the two-layer system to a forcing applied below the level of the nudging. Below the nudging region, the response consists of the full, physical response [i.e., that described by (10) with values appropriate to the free layer], plus a correction to the zonal wind

$$\rho_0 u_2' = \rho_0(z_N) U_F^- \exp\left(\frac{\Lambda_F^+|z - z_N|}{H}\right) D_- \exp\left(\frac{\Lambda_F^+|z_f - z_N|}{H}\right), \tag{32}$$

where

$$D_- = \frac{(i\omega + \alpha_N)\Lambda_N^+ - (i\omega + \alpha_F)\Lambda_F^+}{(i\omega + \alpha_F)\Lambda_F^- - (i\omega + \alpha_N)\Lambda_N^+}, \tag{33}$$

and similar corrections to the temperature and vertical velocity. For completeness, the full response above the nudging boundary has the form

$$u' = U_N^+ \exp\left(\frac{\Lambda_N^+|z - z_N|}{H}\right) D_+ \exp\left(\frac{\Lambda_F^+|z_f - z_N|}{H}\right), \tag{34}$$

where

$$D_+ = \frac{(i\omega + \alpha_N)(\Lambda_N^- - \Lambda_N^+)}{(i\omega + \alpha_F)\Lambda_F^- - (i\omega + \alpha_N)\Lambda_N^+}. \tag{35}$$

The correction within the free region is the same as that described by Shepherd et al. (1996) when $A = 1$ but includes the possibility of the thermal relaxation rate varying across the interface between the free and the nudged regions. The qualitative behavior does not differ, with the nudging acting to damp zonal wind and temperature anomalies associated with the upward-closing circulation cell created by the forcing, thus inducing an artificial mass circulation near the top of the free region, as can be seen by comparing (32) with (10b). This feedback will tend to damp the zonal wind response but also will produce a secondary temperature response of the opposite sign as the response local to the level of the forcing. The strength of this artificial feedback is controlled by the parameter D_-, which tends to

$$D_- = \frac{-(1/2)A(\sqrt{1 + 4b_n K_N} - 1)}{1 + (1/2)A(\sqrt{1 + 4b_n K_N} - 1)}. \tag{36}$$

in the steady-state limit [cf. (9) of Shepherd et al. (1996)]. This tends to -1 as A or $b_n K_N$ gets large.

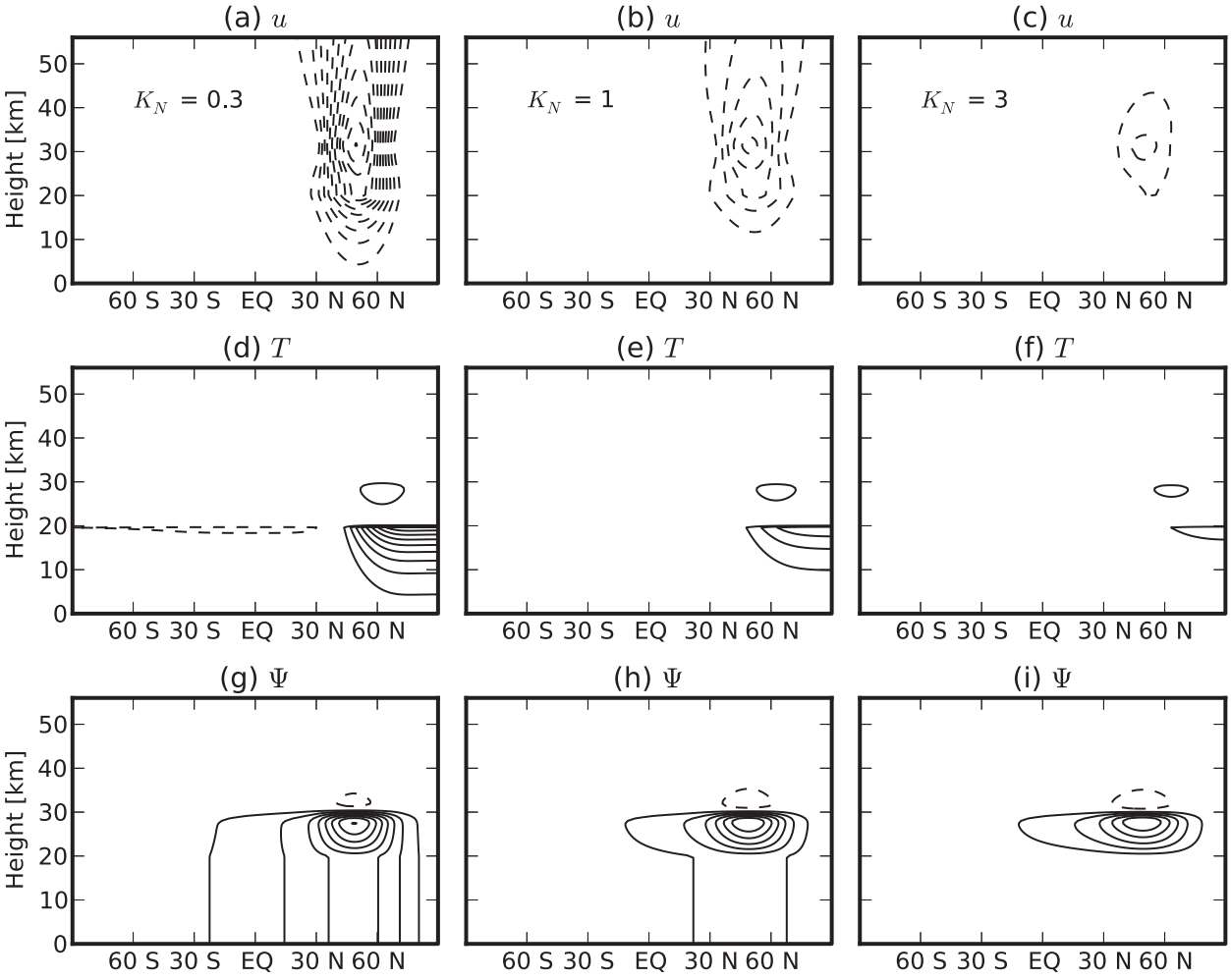

FIG. 2. Steady-state response to the same extratropical force considered in Fig. 1 in an unbounded atmosphere with a free region ($k = 0$) below $z_N = 20$ km. (a)–(c) Zonal wind, (d)–(f) temperature, and (g)–(i) meridional mass circulation responses with the same contour intervals as in Fig. 1. The thermal relaxation in the free region below is 0.1 day^{-1}.

Note that $C_-(\omega) - D_-(\omega) = 1$. Hence, the artificial response below the level of the nudging is closely related to the confinement of the mass circulation induced by $\mathcal{F}'$ within the nudging layer: the stronger the confinement of the mass circulation within the nudging layer ($C_- \to 0$), the stronger this artificial response within the free layer ($D_- \to -1$). This correspondence holds exactly in steady state, but the frequency dependence of the additional exponential factors differs in the two cases.

An example of this feedback is shown in Fig. 3 for an oscillatory forcing of the same structure and thermal relaxation in the free region as considered above, but with $z_0 = 15$ km, and a period $2\pi/\omega = 30$ days, such that $2\pi\alpha_F/\omega = 3$. The left column of panels in Fig. 3 shows the wind, temperature, and mass circulation response to the forcing in a free atmosphere without any nudging layer, while the center and right columns show the responses for two possible nudging-layer configurations with $k_N = 4\,\text{day}^{-1}$ in both cases, but $\alpha_N = 0.4$ and $4\,\text{day}^{-1}$, corresponding to $A = 10$ and 40 and $K_N = 10$ and 1, respectively. The spurious circulation that arises near the base of the nudging layer at $z_N = 20$ km is apparent in Figs. 3h and 3i, as is the corresponding damping of the wind response and opposite-signed temperature anomaly described by Shepherd et al. (1996).

d. *Nudging with a frictional lower boundary*

Imposing the lower boundary condition of Haynes and Shepherd (1989) and following Haynes et al. (1991), this results in the condition

$$[b_n k_s + S(\partial_t + k)]\frac{u'}{H} - (\partial_t + \alpha)\partial_z u' = 0 \quad \text{at} \quad z = 0, \quad (37)$$

where $S = N^2 H/g$ and k_s specifies the rate of frictional relaxation near the surface; here, k_s is taken to be

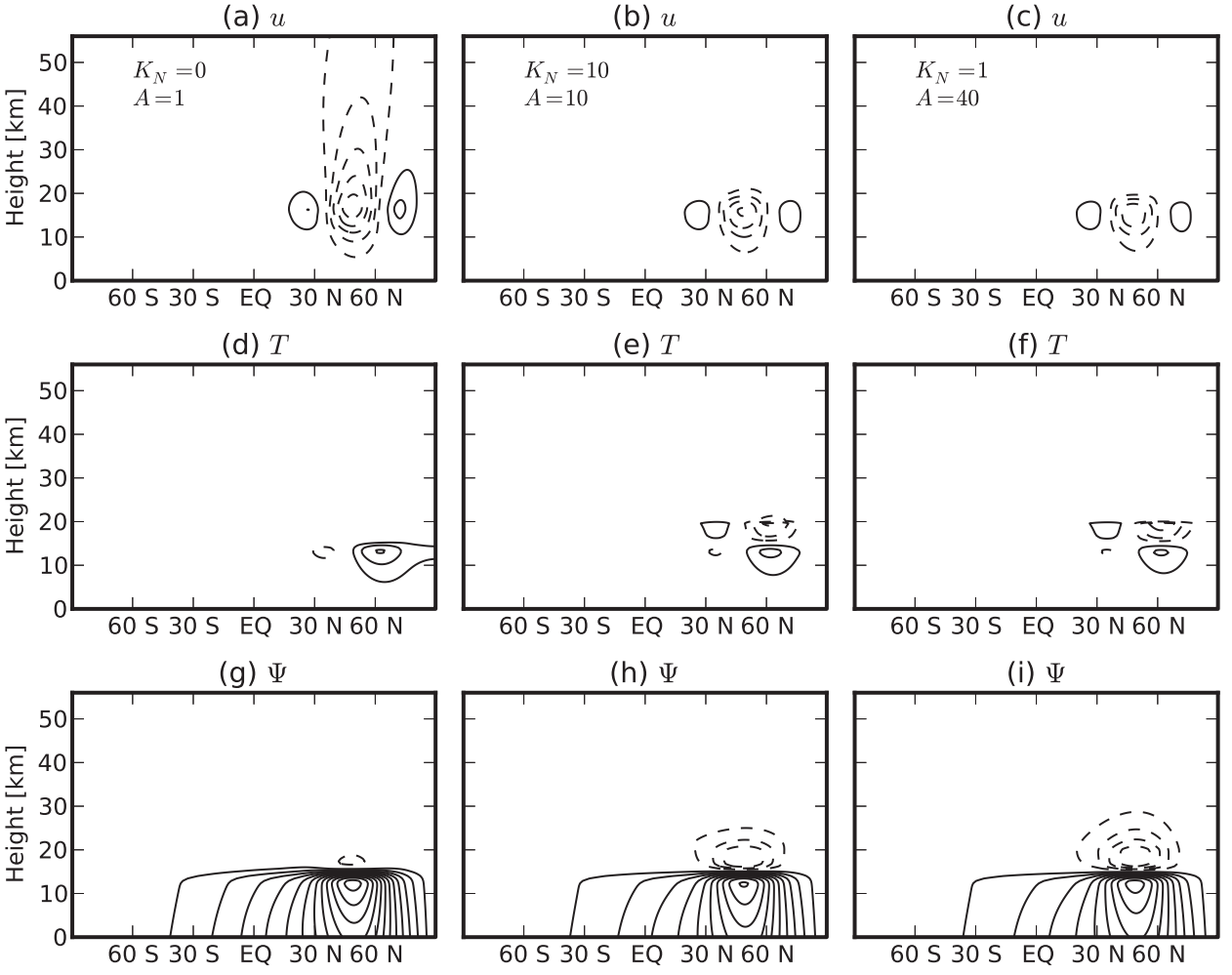

FIG. 3. Response to an oscillatory forcing with a period of 30 days ($\omega = 2\pi/30 \sim 0.2\,\text{day}^{-1}$) of the same amplitude and structure as in Figs. 1 and 2, but now centered at 15 km. (a),(d),(g) The free case in which no nudging is present ($A = 1$, $K_N = 0$). Also, nudged cases with $k_N = 0.5\,\text{day}^{-1}$ where (b),(e),(h) $\alpha_N = 0.4$ and (c),(f),(i) $\alpha_N = 4\,\text{day}^{-1}$, corresponding to $A = 10$ and 40 and $K_N = 10$ and 1, respectively. For all cases, $\alpha_F = 0.1\,\text{day}^{-1}$, as in Fig. 2. The zonal winds and temperatures are shown one-quarter cycle out of phase from the forcing, while the mass circulation is shown in phase with the forcing. The contour intervals are $0.5\,\text{m s}^{-1}$ for the zonal winds, 0.5 K for the temperatures, and $30\,\text{kg m s}^{-1}$ for the mass circulation.

greater than zero. The background relaxation rates in the adjacent region are α and k; in the case considered here, $k = k_F = 0$. The influence of such a layer has been discussed at length by Haynes et al. (1991) and Shepherd et al. (1996), and so we point out only that the frictional lower boundary provides an additional sink for the angular momentum generated by the torque $\mathcal{F}'$. As a consequence, not all of this momentum must be absorbed by the nudging layer in steady state. This has more significant implications for the sponge-layer feedback than it does for the confinement effect.

The confinement of the mass circulation within the nudged layer is controlled in this case by the same exponential factor present in (26) and the parameter

$$C_-^s(\omega) = \frac{C_-}{1 + D_- F e^{-(\Lambda_F^- - \Lambda_F^+) z_N/H}}, \tag{38}$$

$$F = \frac{b_n k_s + i\omega S - (i\omega + \alpha_F)\Lambda_F^-}{b_n k_s + i\omega S - (i\omega + \alpha_F)\Lambda_F^+}, \tag{39}$$

which becomes, in steady state,

$$C_-^s(0) = \frac{1}{1 + (1/2)A(\sqrt{1 + 4b_n K_N} - 1)(1 - F_0 e^{-z_N/H})},$$
$$K_s = k_s/\alpha_F, \tag{40}$$

and $F_0 = 1 - (b_n K_s)^{-1}$. Thus, the confinement of the mass circulation is somewhat less efficient in the presence

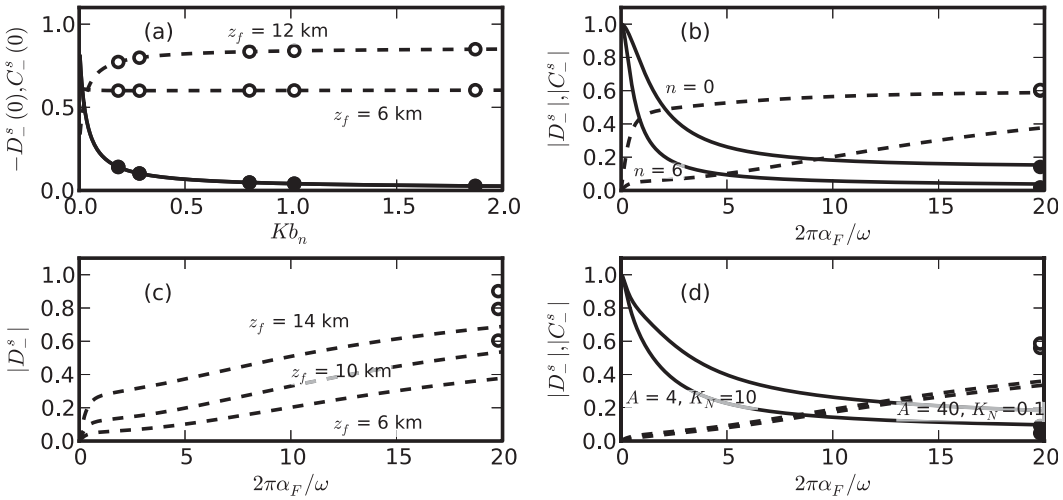

FIG. 4. Factors C^s_- and D^s_- (see text), related to the fraction of the mass circulation that extends below the region of the nudging and the strength of the nudging-layer feedback. (a) Steady-state values, as a function of $K_N b_n$, for $A = 40$ and two values of z_f. Points on each line indicate values obtained when $K_N = 1$. Also frequency dependence as a function of $2\pi\alpha_F/\omega$ (b) dependence on meridional mode n for $A = 40$, $K_N = 1$, $K_s = 25$, and $z_f = 6$ km; (c) dependence of D_- on z_f for $n = 6$, with other parameters as in (b); and (d) frequency dependence for two alternative nudging layer setups for $n = 6$ and $z_f = 6$ km.

of a frictional lower boundary, but the effect decays rapidly as z_N/H increases. Since the time scale for boundary layer friction is much shorter than for radiative relaxation in the troposphere, F_0 is close to unity, and for parameters relevant to HS, the modification to the confinement is less than 1% even for the gravest meridional scales.

The presence of the frictional lower boundary has more important consequences for the nudging-layer feedback, the strength of which is controlled in this case by the parameter

$$D^s_- = D_- \frac{1 - Fe^{-(\Lambda_F^- - \Lambda_F^+)z_f/H}}{1 + D_- Fe^{-(\Lambda_F^- - \Lambda_F^+)z_N/H}} e^{\Lambda_F^+(z_N - z_f)}. \quad (41)$$

The exponential factor has been included in this case because it plays an important role in the transient response that for the sponge-layer feedback occurs much more slowly than the adjustment within the nudging layer.

In steady state,

$$D^s_-(0) = -\frac{(1/2)A(\sqrt{1 + 4b_n K_N} - 1)(1 - F_0 e^{-z_f/H})}{1 + (1/2)A(\sqrt{1 + 4b_n K_N} - 1)(1 - F_0 e^{-z_N/H})}. \quad (42)$$

The lower boundary has a more significant impact on the steady-state limit in this case; in the limit of sufficiently large A or $b_n K_N$ when $D_- \approx -1$ and $F \approx 1$, this becomes simply

$$D^s_-(0) = \frac{1 - e^{-z_f/H}}{1 - e^{-z_N/H}}. \quad (43)$$

Thus, the interaction between the frictional lower boundary and the nudging layer reduces the strength of the sponge-layer feedback for forcings within a scale height or two of the surface, even for regimes in which the confinement of the anomalous mass circulation is essentially complete.

The patterns of behavior of C^s_- and D^s_-, which dictate the strength of the confinement and the sponge-layer effects, respectively, are illustrated in Fig. 4. In all cases C^s_- is shown in solid lines, while D^s_- is shown in dashed lines. Their steady-state forms [see (40) and (43)] are shown in Fig. 4a for the cases $A = 40$ and $K_s = 25$. In both cases, they are purely real, and K_N and b_n arise only in the combination $K_N b_n$, so their values are shown as a function of their product. In this case of $K_N = 1$ (indicated by the symbols), the confinement is nearly complete for all but the first few meridional modes. The influence of the frictional lower boundary is much more significant for the steady-state strength of the sponge-layer feedback; even when the confinement is nearly perfect, the sponge-layer feedback for the case $z_f = 6$ km is reduced by 40%.

The frequency dependence of the modulus of these parameters is presented in Figs. 4b–d, in terms of the product of the radiative time scale and the period of the oscillatory forcing. The corresponding steady state is shown for all curves in Figs. 4b–d by symbols on the right

sides of the plots. For $K_N = 1$, the confinement at $n = 6$ is close to its steady-state strength for forcing periods equal to the thermal relaxation time scale in the free region (Fig. 4b). This confinement reaches its steady-state strength at higher frequencies for shorter meridional length scales; however, at the largest meridional scale ($n = 0$), the steady-state strength is only attained at forcing periods of several multiples of the free thermal time scale. In contrast, the transient adjustment of the sponge-layer feedback is controlled by the additional exponential factor in D^s_-, which approaches its steady state at much higher frequencies for the largest scales (small n) than for smaller meridional scales. This adjustment time scale also depends strongly on the distance of the forcing from the nudging layer, as shown in Fig. 4c.

We close with a brief discussion of what the present analysis has to say about the choice of relaxation rates employed in a nudging layer. The parameters A and K_N discussed to this point are relevant to the nudging layer employed by HS. Figure 4d shows the frequency dependence in the case for two alternative designs of the nudging layer in which the strength of either the thermal or the mechanical nudging is reduced by a factor of 10, corresponding to $A = 4$, $K_N = 10$ and $A = 40$, $K_N = 0.1$. The curves can be compared to the $n = 6$ curves in Fig. 4b. While both choices weaken the steady-state confinement relative to that seen in Fig. 4b, weakening the mechanical relaxation at this meridional length scale has a greater effect on the frequency-dependent adjustment than weakening the thermal relaxation. Neither has a great effect on the transient evolution of the sponge-layer feedback, since for these parameters it is dominated by the additional exponential factor, which depends only on the thermal damping in the free region and the value of $z_N - z_f$; however, in steady state, the trade-off between the strength of the confinement and the strength of the sponge-layer feedback holds. Which of these factors one wishes to optimize will depend on the application in mind.

4. Application to HS experiments

To illustrate the implications of the discussion above for the nudging simulation itself, we consider first an idealized reference simulation, which will in fact exhibit some resemblance to the response obtained by HS. A Gaussian force of the type considered in earlier sections is switched on in an atmosphere with only thermal relaxation. We then consider the behavior of a second simulation, nudged toward the time-dependent response of the idealized reference case. Here, the equations in (2) are solved numerically, using the first 30 Hough modes and a vertical grid from 0 to 80 km at 0.5-km spacing. The thermal relaxation in the free run is set to 0.1 day^{-1}, and the nudging is imposed using equal thermal and mechanical relaxation rates of 4 day^{-1} above 25 km but reduces linearly with height to 0 at 19 km. These nudging parameters closely match those used by HS. The lower boundary condition imposed is that of Haynes and Shepherd (1989), with a frictional lower boundary approximating a delta function with a relaxation rate of 1 day^{-1}. The forcing imposed is of the same form as (21), with $z_0 = 40$ km, $\sigma_z = 3$ km, $\phi_0 = 40°$N, and $\sigma_\phi = 25°$. The amplitude of the forcing is $-10\ \text{m s}^{-1}\ \text{day}^{-1}$.

Since we have been considering the case where the wave driving is felt solely through the eddy terms in the momentum equation, it has been appropriate to associate the meridional circulations with the TEM circulation. In the case of planetary waves that propagate up to the stratosphere prior to breaking, the wave driving will also be associated with significant meridional heat fluxes, which implies the TEM mass circulation will differ from the EM mass circulation in the reference simulation. To illustrate the implications of this for the corresponding mass circulations in the nudged run, we further suppose that the waves responsible for the imposed forcing were produced at the surface of the reference simulation, propagate vertically (with associated meridional heat fluxes) until they reach the altitude of the imposed forcing, then propagate horizontally (implying meridional momentum fluxes) to the dissipation region. The region of the generation is taken to be at a higher latitude than the dissipation region so that the waves propagate equatorward before dissipating. If one takes the lower boundary condition of Haynes and Shepherd (1989) to be relevant for the TEM circulation, then these heat fluxes are irrelevant to the TEM response, but they do define the difference between the EM and the TEM circulations.

We then suppose that the nudged simulation produces no eddies at all, such that $\mathcal{F}_N = 0$. In this case $\mathcal{F}'$ is the negative of the forcing imposed in the reference simulation, and the behavior of the nudged run will be described by the linear superposition of the reference run with the strongly damped response to the anomalous wave driving, as described in previous sections.

The reference solution (FREE), the anomaly (SSW′), and the full-nudged solution (SSW) are shown in Fig. 5, 20 days after the onset of the forcing in FREE, after much of the adjustment described in the appendix has occurred. Figures 5a–c show the wave driving in each case: a patch of westward forcing in FREE, the anomalous eastward forcing in SSW′, and the absence of an external force in SSW. In the reference case, this drives a TEM mass circulation (Figs. 5d–f) that closes predominantly downward

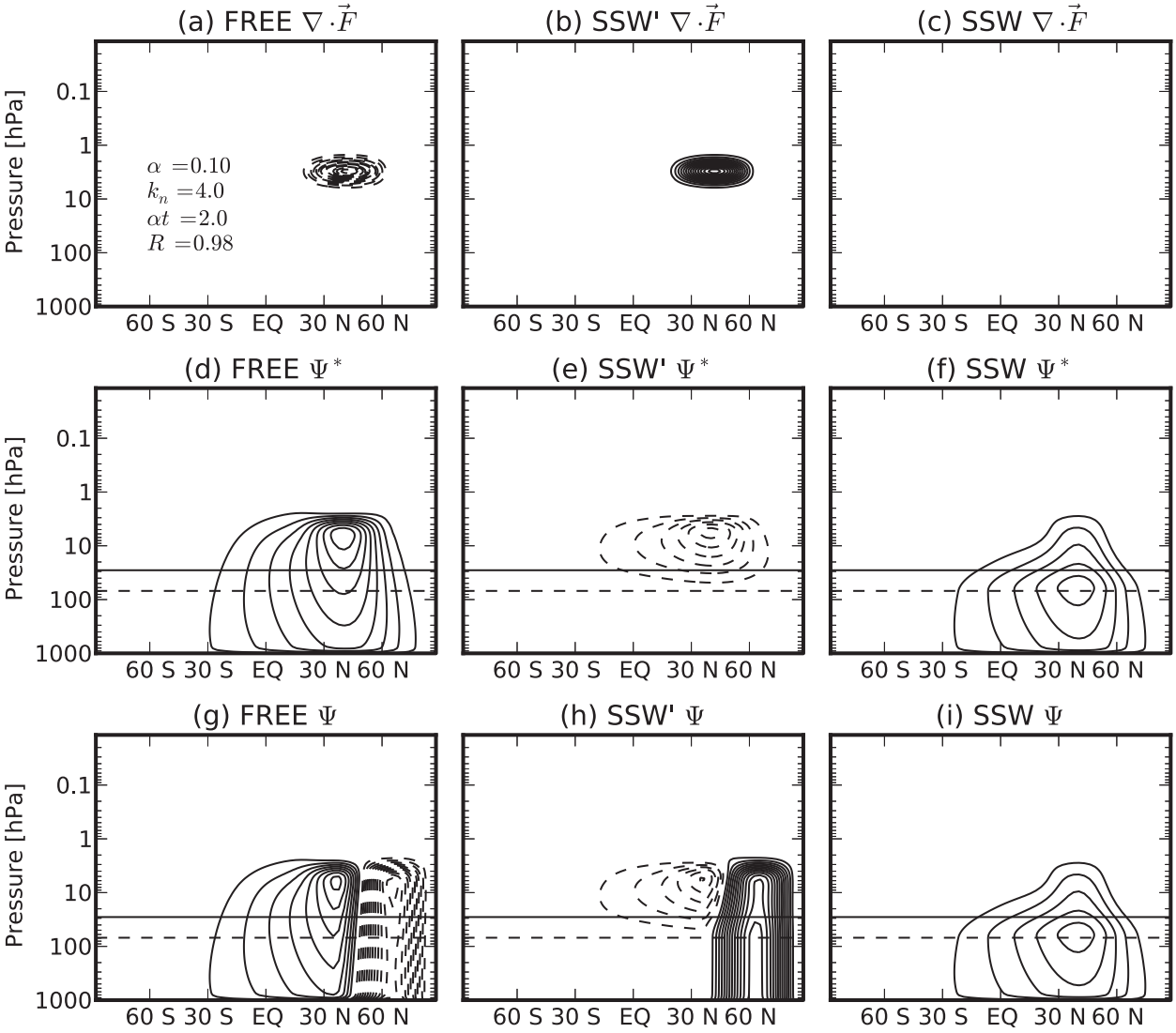

FIG. 5. (a)–(c) Eliassen–Palm flux convergence specified in FREE, SSW′, and SSW cases, with a contour interval of 0.2 m s^{-1} day^{-1}. (d)–(f) TEM and (g)–(i) EM mass streamfunctions; in each case, the contour interval is 0.5 kg m s^{-1}. The solid horizontal line indicates the level above which the nudging is imposed at full strength; its magnitude increases linearly from zero at the dashed horizontal line.

approaching the steady-state limit of a purely downward response. The anomaly response in SSW′, in contrast, is strongly confined within the nudging region, as indicated by the horizontal lines (cf. Fig. 2h). Below the nudging region, where the anomaly response is very weak, the superposition in SSW strongly resembles the reference case, though there is a modest reduction in strength of the meridional circulation. However, within the nudging region, the absence of the wave driving in SSW results in a strongly modified meridional circulation; some poleward circulation is still present within the nudged region, but it is much weaker than in FREE and narrower in latitude. Finally, the EM circulation is shown in Figs. 5g–i for a wave source near 60°N. The offset of the heat fluxes from the EP flux convergence in FREE results in a dipolar circulation cell, with upward and equatorward transport near the pole, and the strongest downward velocities near 50°N. The absence of eddies in SSW implies the opposite-signed fluxes in SSW′; hence, the EM circulation will consist of a high-latitude cell of the opposite sign as that in the FREE case, while the lower-latitude cell remains predominantly within the nudging region. The superposition of the two yields exactly the same circulation structure as in the TEM case, consistent with the absence of any heat fluxes in SSW.

These features can be compared to the TEM and EM mass circulations computed from the simulations described by HS. The reference simulation in this case

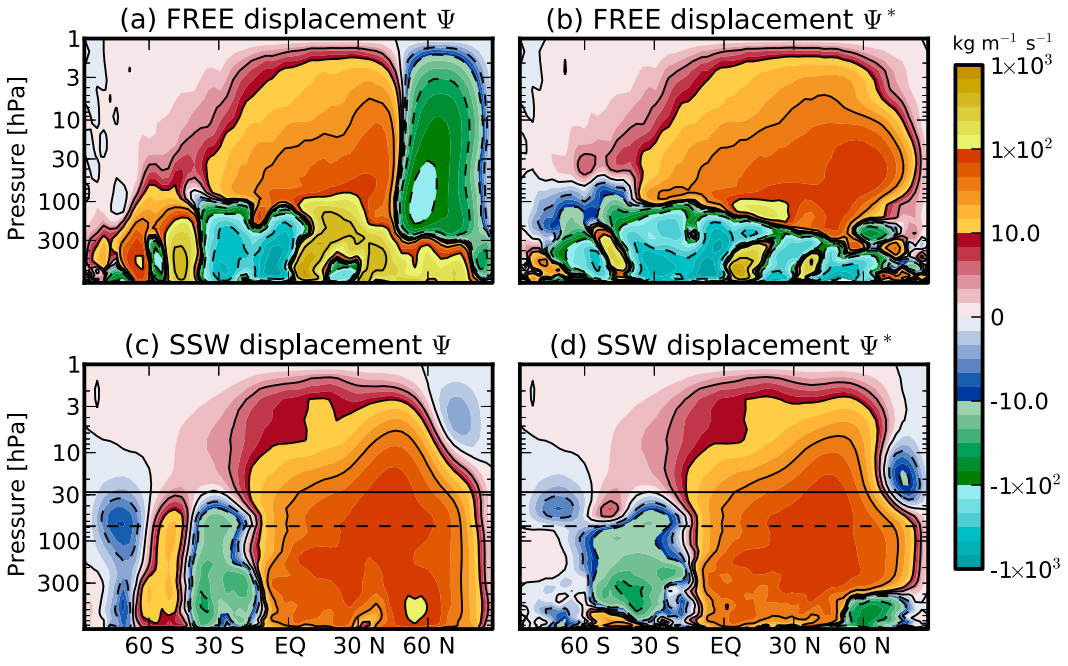

FIG. 6. TEM and EM mass circulation anomalies from the simulations described in HS. See text for description.

(FREE) was a free-running version of the Canadian Middle Atmosphere Model, in particular during a stratospheric sudden warming. The period considered here is a 10-day window during which the wave driving in FREE peaks, inducing the strong deceleration of the stratospheric winds. The nudged simulation in this case is the ensemble average of roughly 100 members, all nudged toward this warming event; while some stratospheric wave driving is present, it is much weaker than in the reference case (see Fig. 3 of HS). Figure 6 shows the EM and TEM mass streamfunctions for the FREE and SSW cases; in both cases these are departures from the climatology of FREE. The stratospheric EM circulation in FREE shows a clear two-celled structure, with peak downward velocities near 50°N, in contrast to the single-celled TEM circulation, which shows a single equator-to-pole cell. In contrast, the EM and TEM mass circulations in SSW do not differ strongly within the stratosphere, consistent with the weak departure from climatological wave driving present at this point in the nudged SSW ensemble. Moreover, the narrowed meridional extent of the circulation within the nudged layer closely resembles the structures predicted by the idealized calculations seen in Figs. 5f and 5i.

The tropospheric meridional circulation is dominated by the response to the tropospheric eddies, which will not be the same in the single instance of FREE and the ensemble-averaged SSW; hence, below the region of the nudging the net meridional circulation of SSW will not match that of FREE. To evaluate the tropospheric influence of the nudged stratosphere, we must rely on an offline diagnosis of the circulation. An estimate of the Coriolis torques induced by the stratospheric wave driving (both resolved and parameterized) in FREE and in SSW is presented in HS (their Fig. 4).

To estimate the magnitude of the anomalous tropospheric torques in SSW, we model the anomalous wave driving responsible for the warming in the reference run by two pulses, with the spatial extent again given by (21) and the temporal evolution given by

$$\begin{cases} \sin^2\left[\dfrac{\pi(t-t_0)}{\sigma_t}\right], & \text{if} \quad t_0 < t < t_0 + \sigma_t \\ 0, & \text{otherwise}, \end{cases} \tag{44}$$

and with parameters specified in Table 2. These parameters were chosen to roughly match the spatial structures of the anomalous EP flux convergences at the end of January and February, respectively, which can be seen in Fig. 3 of HS. However, the aim here is not to quantitatively reproduce the anomalous wave driving in the HS experiments, but rather to demonstrate the character of the response. The anomalous tropospheric Coriolis torques that would be produced by the absence of this wave driving are shown in Fig. 7a. The anomalous torques are essentially confined to when the forcing anomaly is active in the stratosphere and vanish when the forcing ends. This is consistent with the rapid diabatic adjustments that confine the anomalous circulation within the nudging layer. The signal is thus essentially

TABLE 2. Parameters for the idealized forcings used in Fig. 7a (first two rows) and Figs. 7b and 7c (third row).

Pulse	f'_n [(m s^{-1}) day^{-1}]	t_0	σ_t (days)	z_0 (km)	σ_z (km)	ϕ_0 (°)	σ_ϕ (°)
Stratosphere 1	1000	26 Dec	6	40	12	55	30
Stratosphere 2	120	26 Jan	10	25	8	65	25
Troposphere	−4	1 Dec	60	7.5	2	55	20

the Eliassen adjustment to the wave driving and can also be seen from the top curves in Fig. 4b, which show that the confinement is nearly complete for all but the largest meridional modes by a single radiative time scale. Since the Eliassen adjustment well below the level of the forcing is smaller than the full diabatic adjustment, one can expect that the tropospheric Coriolis torques induced by the stratospheric forcings in the nudged experiments of HS will closely match those of the reference simulation, up to small departures coincident with periods of strong stratospheric wave driving. This can be seen in Fig. 4 in HS.

As discussed above, however, one consequence of this strong confinement is the presence of a significant sponge-layer feedback. This also cannot be directly diagnosed from the model output, so we take a similar approach to estimating the magnitude of this effect. We model the anomalous tropospheric EP flux convergences associated with the fluxes shown in Figs. 9 and 10 in HS with a pulse of forcing of the same structure, with parameters specified in Table 2. To estimate the size of the feedback, the response to this wave driving has been computed in a free atmosphere with a frictional lower boundary but no nudging, and in an equivalent atmosphere with a nudging layer. The tropospheric wind anomalies at 60°N in the free atmosphere are shown in Fig. 7b, and the anomalous response of the atmosphere with a nudging layer is shown in Fig. 7c; note that the contour intervals in the latter plot are an order of magnitude smaller than those in the former plot. The effect is most noticeable close to the base of the nudging layer but represents only a small perturbation to the flow. Note that the analysis of the previous section shows that in steady state, far from the surface, one expects the size of the effect to be commensurate with the strength of the confinement; that is, it would produce anomalies of the same magnitude as the free response. Two effects are essential for limiting the size of this feedback. First, in the presence of the frictional lower boundary, the strength of the feedback is attenuated by proximity to the surface, which, in steady state, corresponds to a 30% reduction relative to the unbounded case [cf. (43) and Fig. 4a]. Second, there is a time scale $(z_N - z_f)/W_F$ for the feedback to be established after the onset of the tropospheric wave driving associated with the propagation of the adjustment front from the level of the forcing, up to the base of the nudging layer, where $W_F = H\alpha_F/b_n$ is the speed of the adjustment front in the free layer [see the appendix and Shepherd et al. (1996)]. Since the idealized forcing does not project strongly onto the gravest meridional modes, and since the time scale of the forcing is no more than a few radiative time scales, the feedback has not reached its steady-state strength. This time scale for the feedback to reach full strength is also illustrated in Fig. 4c.

The idealized approximation of the tropospheric eddy flux convergence used here is considerably cruder than the stratospheric cases considered above; nonetheless, since the base of the nudging region is at least a scale height away from the top of the tropopause, and since the time scale of the tropospheric response is still short compared to the time scale on which the sponge-layer feedback establishes itself, the spurious effects are unlikely to represent more than a weak correction to the

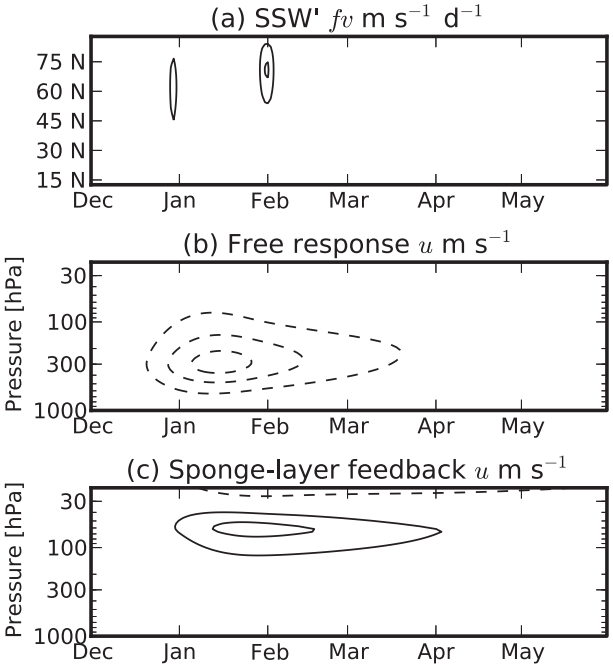

FIG. 7. (a) Idealized estimate of spurious tropospheric Coriolis torques induced by missing stratospheric wave drag. Contour interval is 0.1 m s^{-1} day^{-1} with the zero contour omitted. (b) Idealized free response to a pulse of wave driving in the troposphere. Contour interval is 1 m s^{-1}. (c) Anomaly due to a spurious nudging-layer feedback. Contour interval is 0.1 m s^{-1}. See text and Table 2 for specifications of the idealized forcings.

response obtained by HS. Moreover, the effect would be to reduce the magnitude of the tropospheric response seen in the nudged ensembles, such that it would underestimate the physical response to the stratospheric events.

5. Discussion and conclusions

The present work has focused on the nature of the zonally symmetric dynamics associated with artificially relaxing or nudging a numerical simulation of the atmosphere toward a reference state. Two effects arising from the presence of the nudging have been characterized: the ability of the nudging layer to confine circulations associated with anomalous torques within the nudged region, and the presence of a ''sponge-layer feedback'' (Shepherd et al. 1996) that produces spurious responses to torques below the nudging.

In the quasigeostrophic limit, anomalies in the zonally averaged nudged system are produced by differences between the wave driving in the nudged system and that in the reference system [see (7)]. The anomalies are described by the zonally symmetric system of Plumb (1982) but are subject to the mechanical and thermal relaxation rates imposed by the nudging, in addition to the physical relaxation (such as that due to radiative transfer). Understanding the behavior of these anomalies thus corresponds to the diabatic adjustments described by Haynes et al. (1991), but with finite mechanical relaxation. Although we have been concerned with the presence of a stratospheric nudging layer, this framework could easily be applied to other nudging geometries.

Within the nudging region, far from any boundaries, the steady-state magnitude of the anomalous zonal wind and temperature responses are strongly controlled by the strength of the nudging, in the sense that they tend to be inversely proportional to it. The anomalous meridional circulation, however, is not directly controlled by the nudging and is of the same order as the circulation induced by wave driving in the free system. The response of all fields (or their density-weighted counterparts) is subject to exponential decay with a steady-state height scale H_K, which scales with the inverse square root of the ratio of the mechanical and thermal relaxation rates K for all but the largest meridional scales.

If the nudging is only imposed above a given height, the mass circulation induced by the anomalous wave driving is largely confined within the nudging region, with an efficiency C^s_- that increases with the ratio A of the thermal relaxation associated with the nudging to that associated with the radiative transfer. This implies that the nonlocal meridional circulation in the troposphere induced by wave driving in the stratosphere of the reference run will be reproduced up to this small correction even if the wave driving itself is not present in the nudged run. This confinement is diabatic and is largely established on the time scales of the nudging, particularly at smaller meridional scales.

The strength of this confinement is closely related to the strength D^s_- of the sponger-layer feedback, which produces spurious meridional circulations within a scale height or so of the base of the nudging layer in response to forcings below the nudged layer. If both the forcing and the nudged layer are far from the surface, the strength of the sponge-layer feedback is equal in the steady state to the strength of the confinement; however, the sponge-layer feedback is more significantly affected by the presence of a frictional lower boundary and weakens for forcings close to the surface. Because the transient adjustment occurs within the free layer, the time scale required for the spurious circulation to be established is also much longer than that required to establish the confinement, in the case of strong nudging.

The present work has been strongly motivated by the experimental setup of HS in which the zonal-mean state of the stratosphere in a comprehensive stratosphere-resolving GCM has been artificially constrained or ''nudged'' to follow the zonal-mean evolution of a reference sudden warming simulated by the same model. In this case the confinement of the anomalous circulation within the stratosphere permits the nudged simulation to reproduce the physical meridional circulations in the troposphere induced by the stratospheric forcings in the reference event. The weak differences apparent in these circulations are essentially associated with the adiabatic component of the zonally symmetric adjustment to the anomalous wave driving in the nudged ensembles.

The strong confinement produced by the particular nudging setup used by HS also implies the potential presence of a strong sponge-layer feedback that would damp the wind response to anomalous tropospheric eddy driving in the nudged ensemble in the lowermost stratosphere. However, the intraseasonal time scales associated with recovery of the stratospheric vortex are not long enough for the spurious circulations to be fully established, and the associated zonal wind and temperature anomalies thus correspond only to a weak correction to the response.

While the analysis has been strongly motivated by HS, these effects will be present in any nudged or assimilated run, to the extent that data assimilation increments can be modeled by a nudging term. Although nudging setups that also relax the zonally asymmetric component of the stratospheric circulation will result in wave driving that more closely resembles that of the reference state, there are potentially still-missing torques. For instance, the effects on the mean from fluxes due to eddies not resolved

by the data assimilation system (or properly described by a parameterization) in a reanalysis will instead be produced directly by increments on the observed mean flow. If these increments produce a balanced correction to the flow, they will not produce the meridional circulation that would correspond to the missing flux divergences. This missing circulation may have consequences for transport.

This framework is also relevant to the zonally symmetric mechanical relaxation sometimes employed to produce a quasibiennial oscillation. However, the dynamics described here are closely related to the strong coupling (through thermal wind balance in the quasigeostrophic limit) of the zonal wind and temperature fields in the extratropics. Since this coupling is much weaker in the tropics, the imposition of a mechanical relaxation within the tropics will not give rise to any significant, nonlocal effects through these types of mechanisms. Although we have not discussed the use of meridionally dependent nudging regions, numerical experiments we have performed with nudging confined to the tropics confirm this claim.

Acknowledgments. PH is supported by an NSERC postdoctoral fellowship and ERC Project 267760-ACCI.

APPENDIX

Transient Adjustment

Since the response to forcings at frequencies that are small compared to the nudging rate will be close to the steady-state form, in a region of strong nudging, one expects this steady-state limit to be reached quite rapidly in response to a transient forcing. It is nonetheless interesting to consider just how this steady state is achieved, in particular since the character of this adjustment changes when $K_N > 1$. We consider here a switch-on forcing, $\mathcal{F}' = f_n'\delta[(z - z_f)/H]\Theta(t)$, within the nudging region. Following Haynes et al. (1991), this can be computed using standard Laplace transform methods:

$$u'(t) = \frac{1}{2\pi i}\int_\Gamma \frac{\hat{u}'(s)}{s} e^{ts}\, ds, \tag{A1}$$

where $\hat{u}'(s)$ is given by replacing $i\omega$ with s in (10) and Γ is the Bromwich inversion contour, which lies to the right of all singularities in the integrand.

The argument of the exponential in the integrand has saddle points where

$$(s_0+\tilde{\alpha})^{1/2}(s_0+\alpha)^{3/2} = (1-K_N)\frac{b_n\alpha^2 Z}{(1+4b_n)^{1/2}}, \quad Z = \frac{|z-z_f|}{H\alpha t}. \tag{A2}$$

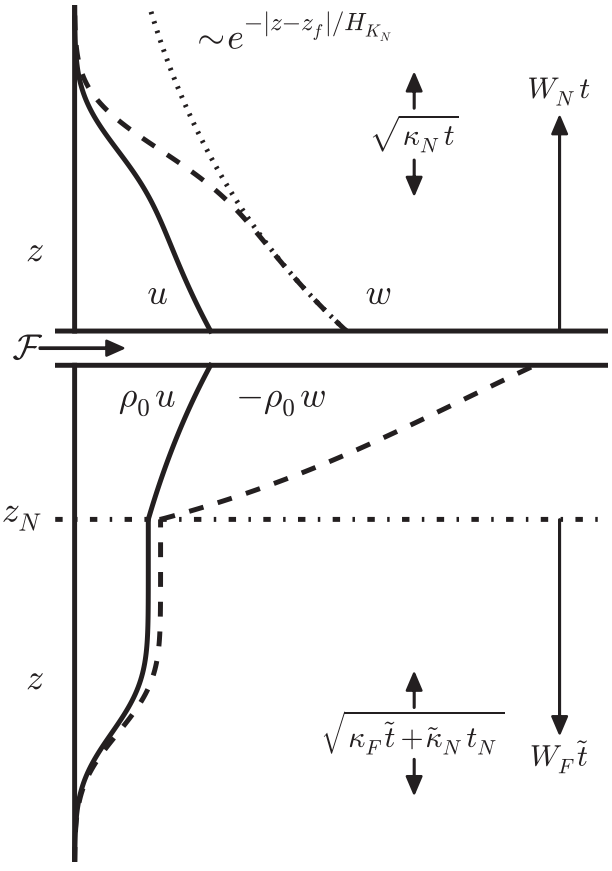

FIG. A1. Schematic diagram of adjustment to a vertically localized forcing (at z_f, indicated by $\mathcal{F}$) with the meridional structure of a Hough mode in a model atmosphere with a nudging region above the dashed–dotted horizontal line, in which the thermal nudging is stronger than the mechanical nudging ($K_N < 1$). Above the forcing, the winds and vertical velocities adjust behind a wave front that propagates upward with velocity W_N and diffusion κ_N. Their value behind the wave front is the contribution that decays in height with e-folding scale H_{K_N} (dotted line). Below the forcing layer, the response will consist of an initial front that propagates downward at the same rate within the nudging layer. When that front reaches the boundary z_N, a secondary wave front subsequently propagates up from the boundary (and past the level of the forcing; this is not indicated in the schematic). Below the boundary, the wave front propagates with speed W_F and κ_F, leaving behind mass-weighted fields that are constant in height. The zonal wind field (solid lines) at all heights is on the order of the inverse of the relaxation rates within the nudging region. In contrast, the vertical velocity (dashed line) is not controlled directly by the nudging just below z_f but is, instead, strongly controlled by the effective boundary condition [(30)], although it does decay in the vertical with H_{K_N}.

Taking a branch cut from $-\tilde{\alpha}$ to $-\alpha$, for $K_N > 1$, this has two solutions along the real axis, one on each side of the branch points. The saddle point of interest is that which lies to the right of the branch points, which passes through the origin at a particular value of $Z \equiv Z_c$. As was

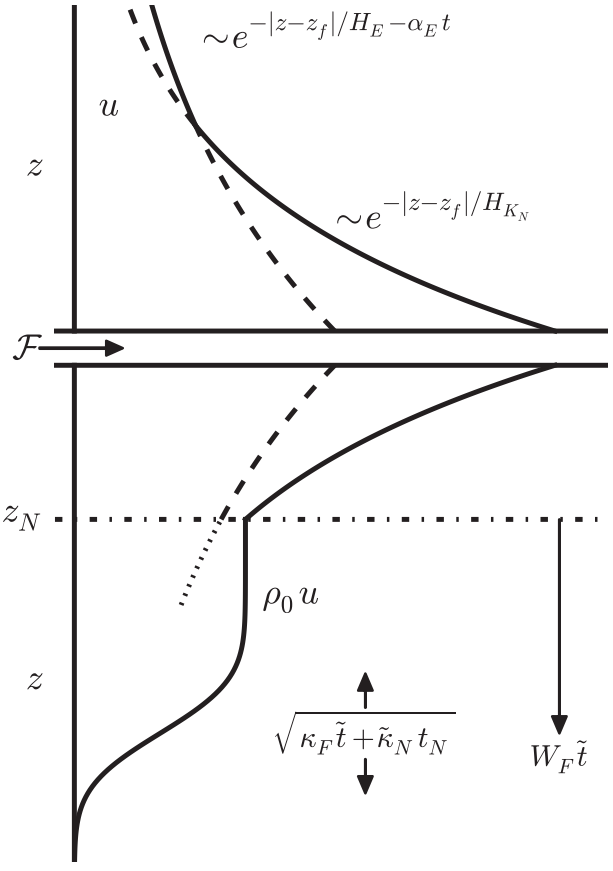

FIG. A2. As in Fig. 8, but for a nudging region in which the mechanical relaxation is stronger than the thermal relaxation ($K_N > 1$). Within the nudging region, the response consists of two components. First, the steady-state response, which emerges immediately after the forcing is switched on, with a vertical e-folding scale of H_{K_N} in the mass-weighted fields below z_f and in the fields themselves above z_f; this contribution dominates near the forcing level. Second, a contribution from the vertical e-folding scale $H_E(>H_{K_N})$ that decays in time at modified thermal relaxation rate α_E, which dominates farther away from z_f. A similar correction will also emerge from the lower boundary of the nudging region, but this contribution is not shown. The exponential decays of these contributions are labeled and are shown by solid lines where they dominate the full zonal wind response and by dashed lines where they do not. Sufficiently far below the level of the nudging, the adjustment resembles that in the free layer described in Fig. 8. The adjustment near z_N at intermediate time scales will involve a more complicated transition from the adiabatic structure (which is only weakly aware of the boundary between the two regions) to the steady state.

argued by Haynes et al. (1991), one can expect the transition from the initial state to the steady-state limit to occur near this value Z_c. Following their methodology, one finds in the limit of large αt but $Z \approx Z_c$ that

$$u' = \frac{\hat{u}'(0)}{2}\,\mathrm{erfc}\left(\frac{|z - z_f| - Wt}{2\sqrt{\kappa t}}\right), \qquad \text{(A3)}$$

above z_f, with a similar expression holding for $\rho_0 u'$ below the level of the forcing. The complementary error function erfc(x) is defined as in Haynes et al. (1991) such that it vanishes as x tends to positive infinity and approaches 2 as x tends to negative infinity. This describes the transition from the resting state to the steady-state solution as occurring at a wave front that travels away from the forcing level with speed,

$$W(K) = \frac{H\alpha}{b_n}\frac{(1 + 4b_n K)^{1/2}}{1 - K}, \quad W_N = W(K_N), \qquad \text{(A4)}$$

and broadens at a rate corresponding to diffusivity:

$$\kappa(K) = \frac{H^2\alpha}{b_n^2}\frac{1 + (1 + 3K)b_n}{(1 - K)^2}, \quad \kappa_N = \kappa(K_N). \qquad \text{(A5)}$$

This adjustment is qualitatively very similar to that described in Fig. 3 of Haynes et al. (1991), though at nonzero values of K_N the steady-state response above and density-weighted response below are no longer constant with height, and since the steady-state vertical velocity is nonzero above the level of the forcing, its adjustment resembles that of the zonal winds.

As K_N approaches 1, both W_N and κ_N tend to infinity, indicating that the steady state is reached extremely quickly. At $K_N = 1$, $\Lambda^{\pm}$ values no longer depend on s. In this case the structure of the steady-state meridional circulation response to the imposed forcing is attained instantaneously (since the temperature changes induced by the thermal relaxation are in thermal wind balance with the wind changes induced by the mechanical relaxation). Since the Coriolis torque and adiabatic heating terms do not vary with time, the zonal winds and temperatures simply grow in place until the relaxation terms balance the combination of the applied force and the meridional circulation response.

In the limit that the forcing is many scale heights away from the level of the nudging, the transient response to a switch-on forcing involves an initial adjustment within the nudging region. When the wave front reaches the boundary of the two regions, a pair of secondary wave fronts emerge. One propagates back into the nudging region (with the same speed and diffusion), behind which the steady-state limit of the corrections discussed in section 3b remains. Below the nudging layer, the wave front travels downward in the free region with speed W_F and diffusion κ_F, with a small correction to account for the time it takes for the initial wave front to reach the boundary z_N:

$$\rho_0 u' = \frac{f_n' b_n}{2\alpha_F}\,\mathrm{erfc}\left(\frac{|z - z_N| - W_F\tilde{t}}{2\sqrt{\kappa_F\tilde{t} + \tilde{\kappa}_N t_N}}\right), \quad \tilde{t} = t - t_N,$$

$$t_N = \frac{z_f - z_N}{W_N}, \quad \text{and} \quad \tilde{\kappa}_N = \frac{W_F^2}{W_N^2}\kappa_N. \tag{A6}$$

As K_N tends to 1, the adjustment within the nudging layer will occur very rapidly. The case $K_N < 1$ is illustrated schematically in Fig. A1.

Though the steady-state response when $K_N > 1$ does not differ qualitatively from that discussed above, the nature of the transient approach does. In contrast to the case with weak mechanical relaxation, the adiabatic, Eliassen response has a longer vertical length scale than the steady-state response ($H_E > H_K$). Sufficiently far from the level of the forcing, one might then expect an initial Eliassen-like response, which is larger than the steady-state response, and then some kind of adjustment back toward the steady state.

In this case (A2) yields a complex-conjugate pair of saddle points above and below the real axis. The singularity in the argument of the exponential at $-\alpha$ lies closer to the origin than does the branch point at $-\tilde{\alpha}$; hence, Γ in (A3) can be deformed for any time $t > 0$ around the pole at the origin, along the real axis toward $-\alpha$, and then along the lines of stationary phase connecting $-\alpha$ and the saddle points. The steady-state contribution arises from the residual of the pole at the origin, and the adiabatic component of the response arises from the saddle-point contributions. Some insight can be gained by considering the small time limit in which Z is large and from (A2), $|s_0| \gg \alpha, \tilde{\alpha}$. Setting the origin at z_f, one then finds

$$s_0 \approx -\frac{3\alpha + \tilde{\alpha}}{4} \pm i\sqrt{\frac{|z|}{|W|t}}, \quad \text{if}$$

$$|Z| \gg \frac{[1 + (3 + K)b_n]^2}{b_n(1 + 4b_n)^{3/4}(K - 1)}. \tag{A7}$$

To leading order in s_0, the contribution to (A3) from the saddle points becomes

$$u'_{\mathrm{sp}} = \frac{f_n'}{\sqrt{\pi}}\left[(K - 1)\frac{|z|}{H}\right]^{-3/4}\left(\frac{b_n}{1 + 4b_n}\alpha t\right)^{1/4} \times \exp\left(-\alpha_E t - \frac{|z|}{H_E}\right)\sin[\phi(|z|, t)], \tag{A8}$$

$$\phi = \frac{\pi}{4} + \sqrt{(K - 1)\frac{b_n}{1 + 4b_n}\frac{|z|}{H}\alpha t}. \tag{A9}$$

To this order, this contribution decays in height with the Eliassen scale H_E and in time with the modified rate $\alpha_E = (1/4)(3\alpha + \tilde{\alpha}) = \alpha[1 + (3 + K)b_n](1 + 4b_n)^{-1}$, which is faster than the thermal relaxation rate for all $K > 1$. As Z increases, this saddle-point contribution decays relative to the contribution from the pole. At some finite value of Z, the latter becomes dominant and the steady state is reached.

The initial adjustment within the nudging layer comprises a steady-state contribution with vertical scale H_{K_N} decaying away from the forcing, and a contribution with a vertical scale H_E, whose structure resembles the adiabatic response but decays in time with the modified radiative time scale α_E. A secondary contribution will also arise from the presence of the interface between the two layers, but, within the nudging layer, this adjustment occurs very quickly for any K_N significantly greater than 0. Sufficiently far below z_N, (A6) still holds despite t_N becoming negative. At intermediate times near the boundary of the nudging layer, the adjustment will be more complicated as it transitions from the adiabatic response (which can only be weakly aware of the different diabatic properties of the two layers) to the longer time-scale adjustment. The adjustment in this case is illustrated schematically in Fig. A2.

REFERENCES

Alexandru, A., R. de Ella, R. Laprise, L. Separovic, and S. Biner, 2009: Sensitivity study of regional climate model simulations to large-scale nudging parameters. *Mon. Wea. Rev.,* **137,** 1666–1686, doi:10.1175/2008MWR2620.1.

Bielli, S., H. Douville, and B. Pohl, 2010: Understanding the West African monsoon variability and its remote effects: An illustration of the grid point nudging methodology. *Climate Dyn.,* **35,** 159–174, doi:10.1007/s00382-009-0667-8.

Douville, H., 2009: Stratospheric polar vortex influence on Northern Hemisphere winter climate variability. *Geophys. Res. Lett.,* **36,** L18703, doi:10.1029/2009GL039334.

Dunkerton, T. J., 1989: Body force circulations in a compressible atmosphere: Key concepts. *Pure Appl. Geophys.,* **130,** 243–262, doi:10.1007/BF00874458.

Eliassen, A., 1951: Slow thermally or frictionally controlled meridional circulation in a circular vortex. *Astrophys. Norveg.,* **5,** 19–60.

Eyring, V., and Coauthors, 2013: Overview of IGAC/SPARC Chemistry-Climate Model Initiative (CCMI) community simulations in support of upcoming ozone and climate assessment. *SPARC Newsletter,* No. 40, Stratosphere-troposphere Processes And their Role in Climate Project, WMO, 48–66. [Available online at http://www.sparc-climate.org/fileadmin/customer/6_Publications/Newsletter_PDF/40_SPARCnewsletter_Jan2013_web.pdf.]

Garcia, R. R., 1987: On the mean meridional circulation of the middle atmosphere. *J. Atmos. Sci.,* **44,** 3599–3609, doi:10.1175/1520-0469(1987)044<3599:OTMMCO>2.0.CO;2.

Hartley, D. E., J. T. Villarin, R. X. Black, and C. A. Davis, 1998: A new perspective on the dynamical link between the stratosphere and troposphere. *Nature,* **391,** 471–474, doi:10.1038/35112.

Haynes, P. H., and T. G. Shepherd, 1989: The importance of surface pressure changes in the response of the atmosphere to zonally-symmetric thermal and mechanical forcing. *Quart. J. Roy. Meteor. Soc.,* **115,** 1181–1208, doi:10.1002/qj.49711549002.

——, C. J. Marks, M. E. McIntyre, T. G. Shepherd, and K. P. Shine, 1991: On the ''downward control'' of extratropical diabatic circulations by eddy-induced mean zonal forces. *J. Atmos. Sci.,* **48,** 651–678, doi:10.1175/1520-0469(1991)048<0651:OTCOED>2.0.CO;2.

Held, I. M., and M. J. Suarez, 1994: A proposal for the intercomparison of the dynamical cores of atmospheric general circulation models. *Bull. Amer. Meteor. Soc.,* **75,** 1825–1830, doi:10.1175/1520-0477(1994)075<1825:APFTIO>2.0.CO;2.

Hitchcock, P., and T. G. Shepherd, 2013: Zonal-mean dynamics of extended recoveries from stratospheric sudden warmings. *J. Atmos. Sci.,* **70,** 688–707, doi:10.1175/JAS-D-12-0111.1.

——, and I. R. Simpson, 2014: The downward influence of stratospheric sudden warmings. *J. Atmos. Sci.,* **71,** 3856–3876, doi:10.1175/JAS-D-14-0012.1.

Hoskins, B., R. Fonseca, M. Blackburn, and T. Jung, 2012: Relaxing the tropics to an observed state: Analysis using a simple baroclinic model. *Quart. J. Roy. Meteor. Soc.,* **138,** 1618–1626, doi:10.1002/qj.1881.

Jung, T., M. J. Miller, and T. N. Palmer, 2010: Diagnosing the origin of extended-range forecast errors. *Mon. Wea. Rev.,* **138,** 2434–2446, doi:10.1175/2010MWR3255.1.

Morgenstern, O., and Coauthors, 2010: Review of the formulation of present-generation stratospheric chemistry-climate models and associated external forcings. *J. Geophys. Res.,* **115,** D00M02, doi:10.1029/2009JD013728.

Plumb, R. A., 1982: Zonally symmetric Hough modes and meridional circulations in the middle atmosphere. *J. Atmos. Sci.,* **39,** 983–991.

Polvani, L. M., and P. J. Kushner, 2002: Tropospheric response to stratospheric perturbations in a relatively simple general circulation model. *Geophys. Res. Lett.,* **29,** 1114, doi:10.1029/2001GL014284.

Shepherd, T. G., and T. A. Shaw, 2004: The angular momentum constraint on climate sensitivity and downward influence in the middle atmosphere. *J. Atmos. Sci.,* **61,** 2899–2908, doi:10.1175/JAS-3295.1.

——, K. Semeniuk, and J. N. Koshyk, 1996: Sponge layer feedbacks in middle-atmosphere models. *J. Geophys. Res.,* **101,** 23 447–23 464, doi:10.1029/96JD01994.

Simpson, I. R., P. Hitchcock, T. G. Shepherd, and J. F. Scinocca, 2011: Stratospheric variability and tropospheric annular-mode timescales. *Geophys. Res. Lett.,* **38,** L20806, doi:10.1029/2011GL049304.

——, ——, ——, and ——, 2013a: Southern annular mode dynamics in observations and models. Part I: The influence of climatological zonal wind biases in a comprehensive GCM. *J. Climate,* **26,** 3953–3967, doi:10.1175/JCLI-D-12-00348.1.

——, T. G. Shepherd, P. Hitchcock, and J. F. Scinocca, 2013b: Southern annular mode dynamics in observations and models. Part II: Eddy feedbacks. *J. Climate,* **26,** 5220–5241, doi:10.1175/JCLI-D-12-00495.1.

Song, Y., and W. A. Robinson, 2004: Dynamical mechanisms for stratospheric influences on the troposphere. *J. Atmos. Sci.,* **61,** 1711–1725, doi:10.1175/1520-0469(2004)061<1711:DMFSIO>2.0.CO;2.

Taguchi, M., T. Yamaga, and S. Yoden, 2001: Internal variability of the troposphere–stratosphere coupled system simulated in a simple global circulation model. *J. Atmos. Sci.,* **58,** 3184–3203, doi:10.1175/1520-0469(2001)058<3184:IVOTTS>2.0.CO;2.

Thompson, D. W. J., J. C. Furtado, and T. G. Shepherd, 2006: On the tropospheric response to anomalous stratospheric wave drag and radiative heating. *J. Atmos. Sci.,* **63,** 2616–2629, doi:10.1175/JAS3771.1.